19th Australasian Fluid Mechanics Conference
Melbourne, Australia
8-11 December 2014

# Active Drag Reduction of a Simplified Car Model Using a Combination of Steady Actuations

**B.F. Zhang[2], Y. Zhou[1] and S. To[3]**

[1]Institute for Turbulence-Noise-Vibration Interaction and Control
Shenzhen Graduate School, Harbin Institute of Technology, Shenzhen, 518055, China
[2]Department of Mechanical Engineering
The Hong Kong Polytechnic University, Hong Kong SAR, China
[3]Department of Industrial and System Engineering
The Hong Kong Polytechnic University, Hong Kong SAR, China

## Abstract

Active drag reduction of an Ahmed model with a slant angle of 25 º is experimentally investigated based on a combination of steady blowing over the rear window and behind the vertical base. The Reynolds number *Re* examined is $0.9 \times 10^5$ - $2.7 \times 10^5$. Steady blowing $S_1$ was applied along the upper edge of the rear window, which has been demonstrated to be effective in suppressing the recirculation bubble on the slanted surface. This actuation led to a drag reduction up to 12%. Steady blowing $S_2$ was deployed along two side edges of the rear window to break the well-known longitudinal C-pillar vortices, reducing drag by around 6%. Steady blowing $S_3$ and $S_4$ were applied along the upper and lower edges of the base to control the upper and lower recirculation bubbles behind the base to raise the base pressure, producing a drag reduction up to 12% and 15%, respectively. The combination of the four actuations achieved an impressive drag reduction of 25%, greatly higher than any previous drag reduction reported and in fact very close to the target set by automotive industries.

## Introduction

The global warming and fast-climbing oil price in the past few years inspire resurgence in drag reduction research for vehicles. The method of steady blowing has been proven to be effective in delaying or even eliminating two and three-dimensional flow separation [2]. It is also relatively simple from a practical and implementation point of view. Naturally, this method has been widely deployed in studies on the active drag reduction of the Ahmed model.

The wake of an Ahmed model with a slanted surface of 25 º, corresponding to the high drag regime, comprises a separation bubble on the rear window, a pair of longitudinal C-pillar vortices at the side edges of the slanted surface and a recirculation torus behind the vertical base [1]. Controlling the interactions between the three types of coherent structures is the key of drag reduction techniques [5]. Wassen & Thiele [9] numerically deployed streamwise steady blowing along the upper and two side edges of the rear window, and the lower and two side edges of the base, producing a drag reduction by 6.4%. Under such actuation, the upper and lower recirculation bubbles behind the base were considerably enlarged longitudinally, and meanwhile the saddle point behind the bubbles was pushed farther downstream, resulting in a rise in the base pressure by 14%. In their numerical simulation, Bruneau *et al*. [3] used steady blowing through slots on the two side edges of the rear window to impair the C-pillar vortices, achieving 11% drag reduction. Aubrun *et al*. [2] deployed an array of steady microjets along the upper edge of the rear window, blowing normal to the slanted surface, achieving experimentally a drag reduction of 14%. This actuation was shown to be effective to reduce or suppress the recirculation bubble on the rear window, resulting in an increased pressure on the slanted surface.

Previous investigations on active drag reduction have greatly enriched our knowledge in the control of the Ahmed model wake ($\varphi$ = 25°) but also raised a number of issues that have yet to be clarified. Firstly, these efforts have achieved a rather limited success; the maximum drag reduction obtained for this model is only about 14% (Aubrun *et al*. [2]), substantially below the target (30%) set by automotive industries. Most of the previous studies focused on controlling one of the three types of coherent structures in the wake, neglecting the other two and their interactions. In their experimental and numerical investigations on the active drag reduction of an Ahmed model, Brunn *et al*. [4] found that, at $\varphi$ = 35°, the synthetic jet placed at mid of the upper edge of the rear window reduced the separated flow region but at the same time triggered the development of C-pillar vortices; at $\varphi$ = 25°, constant blowing near the two upper corners of the rear window weakened C-pillar vortices but increased the flow separation region. As a result, no significant drag reduction was achieved. Apparently, an effective and efficient active drag reduction technique requires a combination of different actuations schemes, i.e., producing actuations at different locations and orientations, which could not only weaken C-pillar vortices but also increase the pressure over the rear window and the vertical base. Yet, the optimum combination of different actuations for achieving a larger drag reduction remains elusive. As a matter of fact, there have been few studies that deployed a combination of different actuations for the control of an Ahmed body.

This work aims to develop an effective active drag reduction technique for this model. Four different actuations, all based on steady blowing, are investigated. Steady blowing ($S_1$) is arranged along the upper edge of the rear window to suppress the recirculation bubble on the slanted surface. Steady blowing ($S_2$) is deployed along the two side edges of the rear window to break the C-pillar vortices. Steady actuations ($S_3$ and $S_4$) are applied along the upper and lower edges of the base to control the upper and lower recirculation bubbles behind the base to raise the base pressure. The dependence of each individual actuation on the momentum coefficient is examined, along with different combinations of $S_1$, $S_2$, $S_3$ and $S_4$ to maximize drag reduction. The net aerodynamic power saving is also estimated for each actuation scheme.

## Experimental Setup

Experiments were conducted in a closed-circuit wind tunnel at Institute for Turbulence-Noise-Vibration Interaction and Control, Harbin Institute of Technology. The test section of the tunnel is 1.0 m high, 0.8 m wide and 5.6 m long. The flow speed in the test section is uniform to 0.1% and the longitudinal turbulence intensity is less than 0.4%. A flat plate (length × width × thickness = 2.6 m × 0.78 m × 0.015 m) was placed horizontally, 0.1 m from the floor of the test section, with its leading edge 1.5 m downstream of the exit plane of the tunnel contraction. The leading edge of the plate follows a clipper-built curve to minimize flow separation.

A ½-scaled Ahmed model ($\varphi$ = 25°) was placed on the plate, with its front end 0.3m downstream of the plate leading edge. The blockage ratio of the frontal surface of the model to the rectangular test section above the raised floor was around 3.9%. The right-handed Cartesian coordinate system ($x$, $y$, $z$) is defined in figure 1, with the origin $O$ at the midpoint of the lower edge of the model vertical base. The model is 0.522 m in length ($L$), 0.1945 m in width ($W$) and 0.144 m in height ($H$), supported by four cylindrical struts of 15 mm in diameter. The ground clearance between the model underside and the surface of the raised floor was 25 mm.

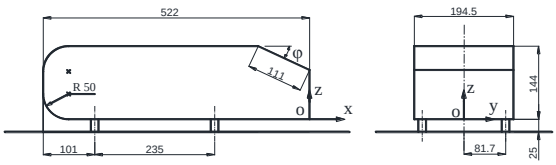


Figure 1. Dimensions of a ½-scaled Ahmed body. The length unit is mm and angle is in degree.

Four different actuations were deployed over the rear window and behind the vertical base of the model for drag reduction. Actuation $S_1$ was produced by an array of microjets long a line 3 mm parallel to and downstream of the upper edge of the rear window. Actuation $S_2$ was generated through slots along the two side edges of the rear window. Actuations $S_3$ and $S_4$ were generated by two arrays of microjets along lines parallel to the upper and lower edges of the base. The momentum coefficient $C_\mu$ of steady actuation is defined by [2, 7]

$$C_\mu = \frac{\rho_{air} Q_j V_j}{0.5 \rho_{air} U_\infty^2 A}, \tag{1}$$

where $Q_j$ and $V_j$ are the volume flow rate and the exit velocity of the jet, respectively, and $\rho_{air}$ is the air density.

Time-averaged drag forces were measured using a six-component aerodynamic force balancer. The balancer is accurate to 0.01 N. The experimental setup is schematically shown in figure 2. The balancer was mounted on a rigid frame which was fixed directly onto the ground in order to avoid the effect of wind tunnel vibration on measurements. The test model was installed on the balancer using 4 hollow cylindrical posts of 280 mm in length and 15 mm in diameter, made from rigid acrylic, which were fixed to a horizontal connecting plate that was screwed onto the balancer. The connecting plate is a lightweight and rigid acrylic plate of 0.3 m × 0.22 m × 0.015 m, with a 0.08 m separation from the bottom wall of the test section. The posts supporting the model were isolated from the raised floor or the wind tunnel wall in order to avoid force transmission. A sealed compartment was installed in the gap between the raised floor and the bottom wall of the test section, enclosing the four supporting posts, so that the posts were not subjected to the aerodynamic forces of the gap flow. Measurements were carried out at $U_\infty$ = 8 - 24 m/s, corresponding to $Re$ = 0.9 × $10^5$ - 2.7 × $10^5$. The sampling frequency was 1 kHz, and the duration was 1 minute, producing a total of 6 × $10^4$ data for each record. At least three records were collected for each test configuration.

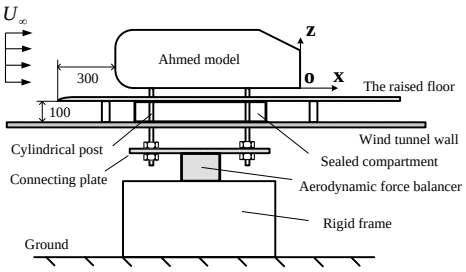


Figure 2. Schematic of drag measurement setup in the HIT experiments. The length unit is mm.

The measured drag was corrected for the thrust forces generated by steady blowing using a method proposed by Littlewood & Passmore [7]. In their experimental study on the active drag reduction of a square-back Ahmed model ($\varphi$ = 0°), the baseline thrust force $F_j$ produced by the steady blowing jet was obtained in quiescent conditions ($U_\infty$ = 0 m/s) and then subtracted from the measured drag forces on the model subjected to incident flow. The drag coefficient $C_D$ is given by

$$C_D = \frac{F_x - F_j}{0.5 \rho_{air} U_\infty^2 A}, \tag{2}$$

where $F_x$ is the drag force measured by the aerodynamic force balancer. Then, the drag coefficient variation $\Delta C_D$ may be calculated by

$$\Delta C_D = \frac{C_D - C_{D0}}{C_{D0}}, \tag{3}$$

where $C_{D0}$ is the drag coefficient of the model without control.

## Characterization of the Base Flow

Figure 3 shows the measured drag coefficient $C_D$ of the Ahmed model in the base flow at different Reynolds numbers $Re$. The drag coefficient exhibits a slight decrease from 0.38 to 0.35 with $Re$ increasing from 0.9 × $10^5$ to 2.7 × $10^5$. The measured drag and its variation agree well with previous studies, as summarized in table 1. For instance, Thacker *et al.* [8] measured using the force balancer a decrease in the drag coefficient of an Ahmed model ($\varphi$ = 25°) from 0.39 to 0.34 as $Re$ was changed from 0.2 × $10^6$ to 1.2 × $10^6$. The small deviation in their $C_D$ from ours could be due to, *inter alia*, a difference in $Re$ and different facilities such as differences in the boundary layer over the raised floor and the surface roughness of the test model between the two investigations.

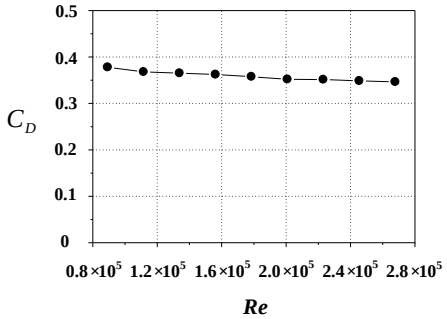


Figure 3 Evolution of the drag coefficient with $Re$.

| Researchers | *Re* | Drag coefficient $C_D$ |
|---|---|---|
| Aubrun *et al*. [2] | 0.3 - 0.6 $\times 10^6$ | 0.41-0.43 |
| Joseph *et al*. [6] | 0.4 - 0.9 $\times 10^6$ | 0.31-0.34 |
| Thacker *et al*. [8] | 0.2 - 1.2 $\times 10^6$ | 0.34-0.39 |
| Present study | 0.09 - 0.27 $\times 10^6$ | 0.35-0.38 |

Table 1 Comparison in the drag coefficient of the Ahmed body ($\varphi$ = 25°) between previous and present measurements.

### Parametric Study of Different Actuations

The four different actuations, i.e., $S_1$, $S_2$, $S_3$ and $S_4$, will be studied in this section. Drag force measurements were conducted at three different Reynolds numbers, i.e. *Re* = 1.3 $\times 10^5$, 1.7 $\times 10^5$ and 2.0 $\times 10^5$. Each individual actuation will be evaluated first to establish its effectiveness in this section before the combination of the four actuations is investigated.

#### Actuation Along the Upper Edge of the Rear Window

Let us examine the effect of the momentum coefficient $C_\mu^{S_1}$ of actuation $S_1$ on the drag coefficient variation $\Delta C_D$. For all the three Reynolds numbers examined, $C_\mu^{S_1}$ shows two critical values at $C_{\mu,c1}^{S_1} \approx 2 \times 10^{-4}$ and $C_{\mu,c2}^{S_1} \approx 1 \times 10^{-2}$ (figure 4). Actuation increases initially the drag at a very low momentum coefficient $C_\mu^{S_1} \leq C_{\mu,c1}^{S_1}$. Once $C_\mu^{S_1}$ exceeds $C_{\mu,c1}^{S_1}$, the drag coefficient decreases rapidly with increasing $C_\mu^{S_1}$ and reaches the minimum at $C_\mu^{S_1} = C_{\mu,c2}^{S_1}$. The maximum reduction of the drag coefficient is about 11% at *Re* = 1.3 $\times 10^5$ and 12% at *Re* = 1.7 $\times 10^5$ and 2.0 $\times 10^5$. However, beyond $C_{\mu,c2}^{S_1}$, the drag starts to rise with increasing $C_\mu^{S_1}$. This observation is consistent with Aubrun *et al*.'s [2] experimental study on the active drag reduction of an Ahmed model ($\varphi$ = 25°) at *Re* = 3.1 $\times 10^5$ - 6.2 $\times 10^5$. They deployed an array of steady microjets at the upper edge of the rear window, achieving a maximum drag reduction of 14% at *Re* = 6.2 $\times 10^5$. A deviation in their maximum drag reduction from our measurement is expected in view of different *Re* and even a possible difference in the details of actuation setup.

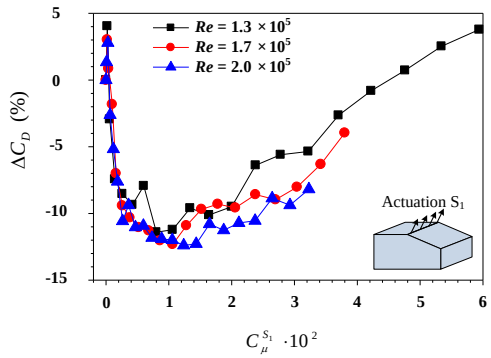


Figure 4 Influence of the momentum coefficient $C_\mu^{S_1}$ of the actuation ($S_1$) on the drag coefficient variation $\Delta C_D$ for different Reynolds numbers.

#### Actuations Along the Two Side Edges of the Rear Window

Figure 5 presents the dependence of the drag coefficient variation $\Delta C_D$ on the momentum coefficient $C_\mu^{S_2}$ of actuation $S_2$. The drag coefficient decreases with increasing $C_\mu^{S_2}$ until reaching a saturation point at $C_{\mu,Sat}^{S_2} \approx 8 \times 10^{-3}$, achieving a maximum drag reduction by 6% at *Re* = 1.3 $\times 10^5$ and 1.7 $\times 10^5$ and 5% at *Re* = 2.0 $\times 10^5$. When the momentum coefficient was increased beyond $C_{\mu,Sat}^{S_2}$, there is no further reduction in drag, and the drag reduction remains at a constant value of about 5%. Bruneau *et al*. [3] showed numerically that steady slot blowing at the two sides of the rear window was effective in breaking the C-pillar vortices through increasing the swirl of vortices and pushing them away to get diffused, and achieved a maximum reduction in drag by 11% at a momentum coefficient of 8 $\times 10^{-3}$ at *Re* = 9.6 $\times 10^3$. The difference in their maximum drag reduction and ours is probably due to the possible boundary and other differences, beside *Re*, between numerical and experimental studies.

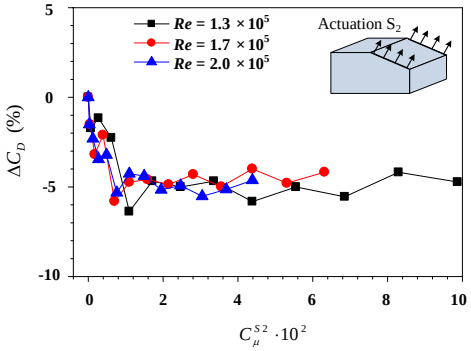


Figure 5 Influence of the momentum coefficient $C_\mu^{S_2}$ of the actuation ($S_2$) on the drag reduction for different Reynolds numbers.

#### Actuation Along the Upper Edge of the Base

Figure 6 presents the effect of the momentum coefficient $C_\mu^{S_3}$ of actuation $S_3$ on the drag coefficient variation $\Delta C_D$. For all the three Reynolds numbers, the drag coefficient decreases with increasing $C_\mu^{S_3}$. At *Re* = 1.3 $\times 10^5$, as $C_\mu^{S_3}$ reaches 0.11, the drag coefficient is substantially reduced by 12%.

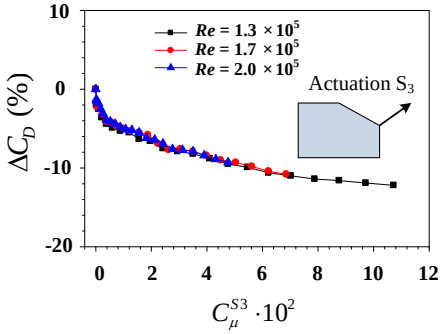


Figure 6 Influence of the momentum coefficient $C_\mu^{S_3}$ of the actuation ($S_3$) on the drag coefficient variation $\Delta C_D$ for different Reynolds numbers

#### Actuation Along the Lower Edge of the Base

Figure 7 shows a variation in $\Delta C_D$ with the increasing momentum coefficient $C_\mu^{S_4}$ of actuation $S_4$. The drag coefficient diminishes with increasing $C_\mu^{S_4}$, down to 15% as $C_\mu^{S_4}$ reaches 0.11 at *Re* = 1.3 $\times 10^5$. In their numerical study at *Re* = 1.6 $\times 10^5$, Wassen & Thiele [10] deployed vertically upward steady blowing along the upper and two side edges of the rear window and 45° inward blowing along the lower and two side edges of the base of an Ahmed model ($\varphi$ = 25°). They found from time-averaged streamlines that steady blowing along the lower edge of the base increased the size of the lower recirculation bubble in the upward direction. Meanwhile, the stagnation point on the base surface was moved upward. As a result, the pressure in the central part of the base was significantly raised by around 30%.

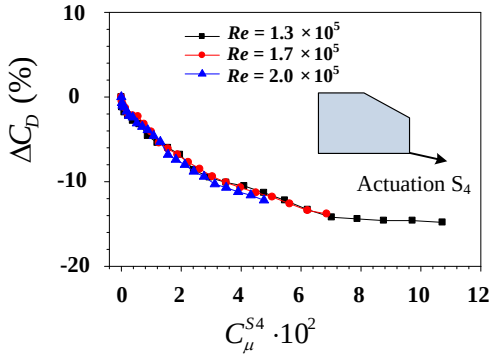


Figure 7 Influence of the momentum coefficient $C_\mu^{S_4}$ of the actuation ($S_4$) on the drag coefficient variation $\Delta C_D$ for different Reynolds numbers

## Combined Actuations

In order to enhance further the drag reduction performance, the combination of $S_1$, $S_2$, $S_3$ and $S_4$ is deployed to control simultaneously the separation bubble and the C-pillar vortices over the rear window and the recirculation bubbles behind the base. Actuations $S_3$ and $S_4$ work at the same momentum coefficient, i.e., $C_\mu^{S_3} = C_\mu^{S_4}$. Figure 8 shows the dependence of the drag coefficient variation $\Delta C_D$, under the combination of $S_1$, $S_2$, $S_3$ and $S_4$, on the momentum coefficient $C_\mu^{S_3+S_4}$ ($= C_\mu^{S_3} + C_\mu^{S_4}$) at $Re = 1.7 \times 10^5$. $\Delta C_D$ decreases with increasing $C_\mu^{S_3+S_4}$, reaching the minimum, 25%, at $C_\mu^{S_3+S_4} = 4.5 \times 10^{-2}$. Above this critical momentum coefficient, $\Delta C_D$ gradually increases for higher $C_\mu^{S_3+S_4}$.

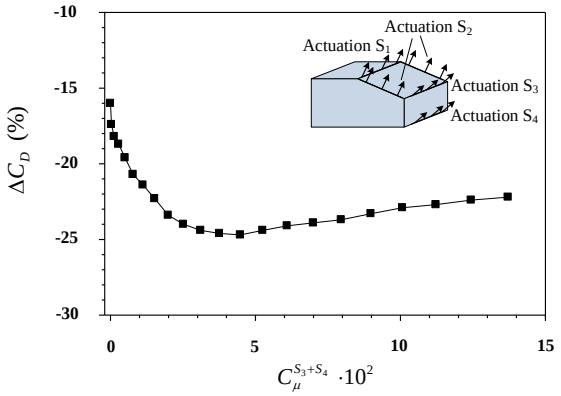


Figure 8 Evolution of the drag coefficient variation $\Delta C_D$ with the combination of actuations ($S_1$, $S_2$, $S_3$ and $S_4$) by varying the summed momentum coefficient $C_\mu^{S_3+S_4}$ for $Re = 1.7 \times 10^5$.

## Conclusions

An experimental parametric study has been conducted on the active drag reduction of an Ahmed model ($\varphi = 25°$) at $Re = 0.9 \times 10^5$ - $2.7 \times 10^5$. Various actuation schemes have been developed, leading to the maximum drag reduction ranging from 5% to 25%, as summarized below.

A substantial maximum drag reduction by 11% - 12% is achieved by steady blowing $S_1$ along the upper edge of the rear window. Under this control, the recirculation bubble over the rear window is reduced. Steady blowing $S_2$ along the two side edges of the rear window produces a maximum drag reduction of 5% - 6% by breaking the C-pillar vortices. The actuation $S_3$ results in a maximum drag reduction of about 11%. The actuation $S_4$ can lead to an upward growth in the size of the lower bubble. As a result, the maximum drag reduction reaches 14% under $S_4$. The combination of $S_1$, $S_2$, $S_3$ and $S_4$ is deployed to control simultaneously the recirculation bubble and the C-pillar vortices over the rear window and the two bubbles behind the base, yielding a maximum drag reduction by about 25%.

## Acknowledgments

YZ wishes to acknowledge support from Research Grants Council of HKSAR through grant GRF 531912 and from Shenzhen City Government through grants JCYJ20130329154125496 and JCYJ20120613134811717.

## References

[1] Ahmed, S.R., Ramm, R. & Faltin, G., Some Salient Features of the Time-averaged Ground Vehicle Wake, SAE paper 840300, 1984, 1-30.

[2] Aubrun, S., McNally, J., Alvi, F. & Kourta, A., Separation Flow Control on a Generic Ground Vehicle Using Steady Microjet Arrays, *Exp. Fluids*, **51**, 2011, 1177-1187.

[3] Bruneau, C., Creusé, E., Delphine, D., Gilliéron, P. & Mortazavi, I., Active Procedures to Control the Flow Past the Ahmed Body With a 25° Rear Window, *Int. J. Aerodynamics.*, **1**, 2011, 299-317.

[4] Brunn, A., Wassen, E., Sperber, D., Nitsche, W. & Thiele, F., Active Drag Control for a Generic Car Model, *Active Flow Control, NNFM*, 95, 2007, 247-259.

[5] Choi, H., Lee, J. & Park, H., Aerodynamics of Heavy Vehicles, *Annu. Rev. Fluid Mech.*, **46**, 2014, 441-468.

[6] Joseph, P., Amandolese, X. & Aider, J.L., Drag Reduction on the 25° Slant Angle Ahmed Reference Body Using Pulsed Jets, *Exps. Fluids*, **52**, 2012, 1169-1185.

[7] Littlewood, R.P. & Passmore, M.A., Aerodynamic Drag Reduction of a Simplified Squareback Vehicle Using Steady Blowing, *Exp. Fluids*, **53**, 2012, 519-529.

[8] Thacker, A., Aubrun, S., Leroy, A. & Devinant, P., Effects of Suppressing the 3D Separation on the Rear Slant on the Flow Structures Around an Ahmed Body, *J. Wind Eng. Ind. Aerodyn.*, **107-108**, 2012, 237-243.

[9] Wassen, E. & Thiele, F., Drag Reduction for a Generic Car Model Using Steady Blowing, AIAA paper 2008-3771, 2008.

[10] Wassen, E. & Thiele, F., Simulation of Active Separation Control on a Generic Vehicle, AIAA paper 2010-4702, 2010.